New Phytologist

Research

Nutrient status regulates MED19a phase separation for ORESARA1-dependent senescence

Steven Le Hung Cheng[1,2], Hui-Wen Wu[1,5], Haiying Xu[1], Reuben Manjit Singh[1], Tao Yao[1,6], In-Cheol Jang[1,2] and Nam-Hai Chua[1,3,4]

[1]Temasek Life Sciences Laboratory, 1 Research Link, National University of Singapore, Singapore 117604, Singapore; [2]Department of Biological Sciences, National University of Singapore, 16 Science Drive 4, Singapore 117543, Singapore; [3]Department of Biochemistry, School of Medicine, National University of Singapore, 8 Medical Drive, Singapore 117596, Singapore; [4]Disruptive & Sustainable Technologies for Agricultural Precision, Singapore-MIT Alliance for Research and Technology, 1 Create Way, #03-06/07/8 Research Wing, Singapore 138602, Singapore; [5]Present address: Diploma in Biotechnology, School of Applied Science, Republic Polytechnic, Woodlands Avenue 9, Singapore 738964, Singapore; [6]Present address: Biosciences Division, Oak Ridge National Laboratory, Oak Ridge, TN 37831, USA

Author for correspondence:
Nam-Hai Chua
Email: chua@rockefeller.edu

Received: *30 May 2022*
Accepted: *16 August 2022*

New Phytologist (2022) **236:** 1779–1795
doi: 10.1111/nph.18478

Key words: liquid–liquid phase separation, mediator complex, nitrogen deficiency, senescence, transcriptional regulation.

Summary

- The mediator complex is highly conserved in eukgaryotes and is integral for transcriptional responses. Mediator subunits associate with signal-responsive transcription factors (TF) to activate expression of specific signal-responsive genes. As the key TF of *Arabidopsis thaliana* senescence, ORESARA1 (ORE1) is required for nitrogen deficiency (−N) induced senescence; however, the mediator subunit that associates with ORE1 remains unknown.
- Here, we show that *Arabidopsis* MED19a associates with ORE1 to activate −N senescence-responsive genes. Disordered MED19a forms inducible nuclear condensates under −N that is regulated by decreasing MED19a lysine acetylation. MED19a carboxyl terminus (cMED19a) harbors a mixed-charged intrinsically disordered region (MC-IDR) required for ORE1 interaction and liquid–liquid phase separation (LLPS).
- Plant and human cMED19 are sufficient to form heterotypic condensates with ORE1. Human cMED19 MC-IDR, but not yeast cMED19 IDR, partially complements *med19a* suggesting functional conservation in evolutionarily distant eukaryotes. Phylogenetic analysis of eukaryotic cMED19 revealed that the MC-IDR could arise through convergent evolution.
- Our result of MED19 MC-IDR suggests that plant MED19 is regulated by phase separation during stress responses.

Introduction

Plants are constantly exposed to various environmental stimuli, both biotic and abiotic stresses, and the mediator complex plays a critical role in stress adaptation through transcriptional regulation (Canet *et al.*, 2012; Lai *et al.*, 2014). One of the most agriculturally relevant abiotic stress is nitrogen deficiency (−N) (Izumi *et al.*, 2010; Have *et al.*, 2017). To avoid −N in the field, fertilizers are ubiquitiously applied (Have *et al.*, 2017); however, such practices negatively impact the environment leading to nitrogen pollution (Imran *et al.*, 2021; Lu *et al.*, 2021), climate change and ultimately global warming (Adviento-Borbe *et al.*, 2013; Lee *et al.*, 2021). Hence, research efforts to uncover the molecular mechanism of how plants respond transcriptionally and adapt to −N are important steps to minimize the environmental impact of agriculture by reducing the reliance on nitrogen fertilizers (Have *et al.*, 2017; Liu *et al.*, 2019; Gramma *et al.*, 2020).

Recently, liquid–liquid phase separation (LLPS) of disordered proteins participating in diverse cellular responses has emerged as a central biological mechanism to compartmentalize several regulatory processes through the formation of biomolecular condensates (Riback *et al.*, 2020; Feng *et al.*, 2021; Lafontaine *et al.*, 2021). During biotic stress, NONEXPRESSOR OF PATHOGENESIS-RELATED GENES 1 (NPR1) undergoes LLPS to form stressed-induced NPR1 condensates to fine-tune cell death and defense response by regulating the protein stability of immune regulators through the ubiquitin–proteasome system (Zavaliev *et al.*, 2020). Under abiotic stress such as high temperatures, EARLY FLOWERING 3 (ELF3) phase separates to positively regulate thermo-responsivity (Jung *et al.*, 2020). The strength of the thermo-responsiveness is positively correlated with the number of glutamine residues in the prion domain of the ELF3 (Jung *et al.*, 2020). Following seed imbibition FLOE1 forms biomolecular condensates to act as a sensor regulating seed germination (Dorone *et al.*, 2021). Likewise, eukaryotic transcriptional apparatus has been demonstrated to regulate gene expression through the formation of nuclear condensates (Hnisz *et al.*, 2017). A well-characterized example is the formation of mammalian MEDIATOR SUBUNIT 1 (MED1) transcriptional condensates associated with super-enhancers (SEs) that regulate

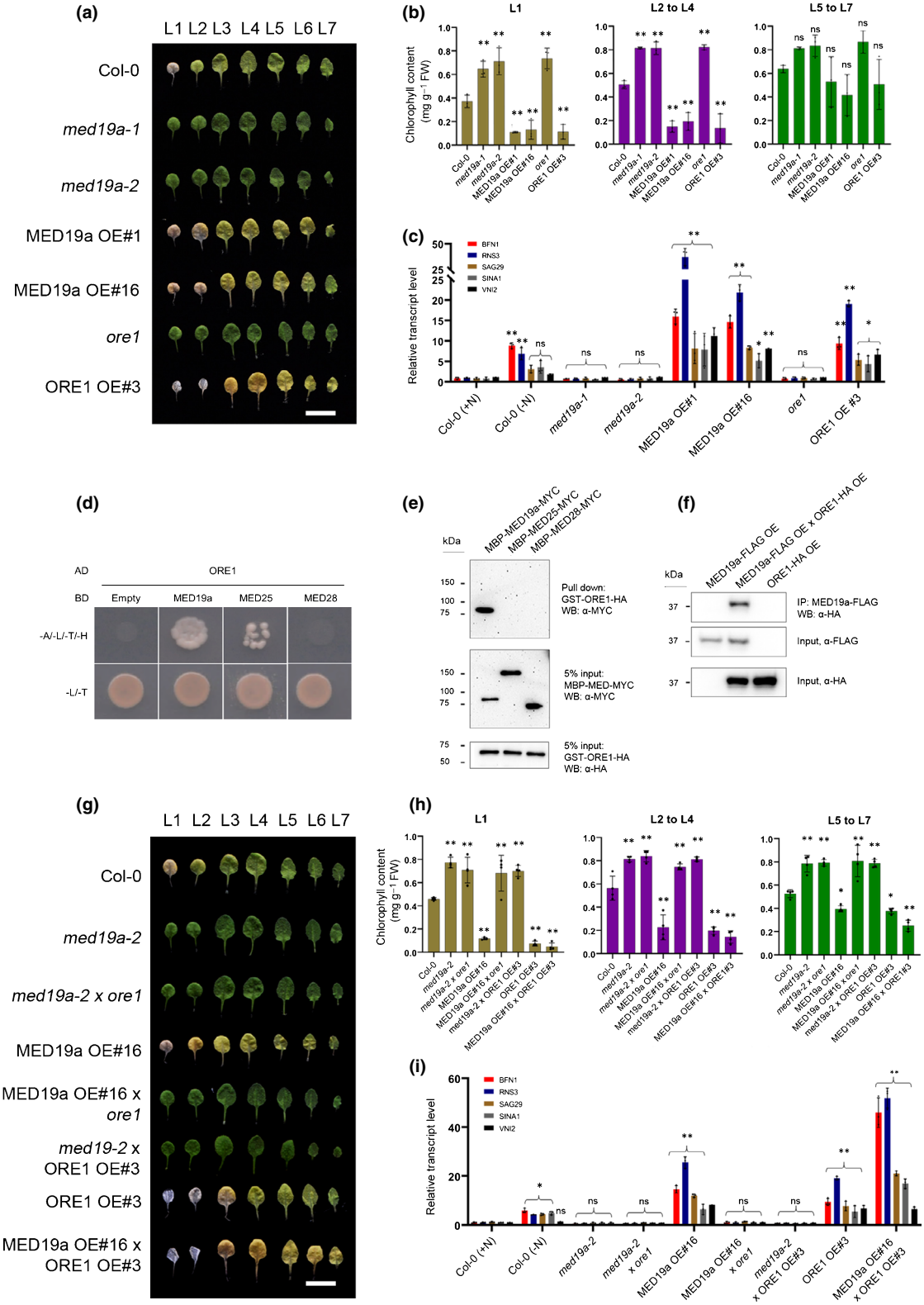

pluriopotency in murine embryonic stem cells (Sabari *et al.*, 2018).

Arabidopsis thaliana ORESARA1 (ORE1) is a NAC (NAM, ATAF and CUC) domain containing transcription factor (TF) (Oh *et al.*, 1997; Woo *et al.*, 2004) which has been shown to be a necessary component of −N induced senescence (Park *et al.*, 2018, 2019). *ORE1* expression is regulated at the transcriptional (Kim *et al.*, 2009), post-transcriptional (Li *et al.*, 2013) and post-

Fig. 1 Arabidopsis MEDIATOR SUBUNIT (MED)19a is a positive regulator of nitrogen deficiency induced senescence by associating with ORESARA1 (ORE1). (a) Nitrogen deficiency (−N) induced senescence phenotype of 17-d-old Arabidopsis plants of the indicated genotypes treated on −N medium for 17 d. OE, overexpression. Bar, 1 cm. (b) Total chlorophyll content in different leaf groups of the indicated genotypes treated on −N medium. L, leaf number. (c) Quantitative reverse-transcription (qRT)-PCR analysis of ORE1 target genes BFN1, RNS3, SAG29, SINA1 and VNI2 of wild-type (WT) (Col-0) treated on nitrogen sufficient (+N) medium and the indicated genotypes treated on −N medium. (d) Yeast-two-hybrid (Y2H) analysis of MED19a, MED25 and MED28 with ORE1. Upper panel, transformed AH109 cells plated on Sabouraud's dextrose (SD)-medium lacking adenine, leucine, tryptophan and histidine (-A/-L/-L/-H). Lower panel, transformed AH109 cells plated on SD medium lacking leucine and tryptophan (-L/-T). Image was taken 2 d after spotting. (e) *In vitro* pull-down assay of various mediator subunits (MED) with ORE1. Upper panel, MBP-MED-MYC proteins pull-down by GST-ORE1-HA via glutathione agarose beads, detected by α-MYC antibody. Middle panel, MBP-MED-MYC proteins 5% input control, detected by α-MYC antibody. Lower panel, GST-ORE1-HA 5% input control detected α-HA antibody. (f) *In vivo* immunoprecipitation analysis of MED19a-FLAG and ORE1-HA in nuclear extracts of Arabidopsis transgenic plants treated with −N medium for 4 d and MG132 for 16 h. Upper panel, ORE1-HA immunoprecipitated by α-FLAG M2 beads, detected by α-HA antibody. Middle panel, loading control, detected by α-FLAG antibody. Lower panel, loading control detected α-HA antibody. (g) Nitrogen deficiency induced senescence phenotype of 17-d-old Arabidopsis plants of the indicated genotypes treated on −N medium for 17 d. Bar, 1 cm. (h) Total chlorophyll content in different leaf groups of the indicated genotypes treated on −N medium. (i) qRT-PCR analysis of ORE1 target genes *BFN1*, *RNS3*, *SAG29*, *SINA1* and *VNI2* of the indicated genotypes treated on +N or −N. (b, c, h, i) Data are means ± SD. $n = 3$ (biologically independent repeats) and individual data points as overlays. ns, no statistical difference. (b, h) Asterisks indicate statistically significant difference compared with Col-0. *, $P < 0.05$; **, $P < 0.01$; one-way ANOVA, Dunnett *post hoc* analysis. (c, i) The expression level of Col-0 (+N) was set at 1. Asterisks indicate statistically significant difference in various genotypes were compared with Col-0 (+N) for each respective gene. *, $P < 0.05$; **, $P < 0.01$; two-way ANOVA analysis, Dunnett *post hoc* analysis.

translational levels (Park *et al.*, 2018, 2019; Durian *et al.*, 2020), reflecting the key roles it plays in plant stress adaptation. For such signal-responsive TFs to execute their functions, it must interact with the mediator complex in order to recruit RNA polymerase II to activate expression of downstream genes (Soutourina, 2018). However, the mediator subunit necessary for ORE1 activity has not yet been identified.

Here, we found that the most disordered *Arabidopsis* mediator subunit, MEDIATOR SUBUNIT 19a (MED19a) undergoes LLPS during −N, but not under nitrogen sufficiency (+N), which is regulated by decreasing MED19a lysine acetylation. MED19a positively regulates −N induced senescence by physically associating with ORE1 through its carboxyl terminus mixed-charged intrinsically disordered region (MC-IDR). Using biochemical, genetic and complementation analyses, we demonstrated that the MED19 MC-IDR, found in both plants and metazoans, is sufficient to promote LLPS *in vitro* and interacts with ORE1 through various weak multivalent interactions contributed by the enriched residues in MC-IDR. We provide evidence that MC-IDR could arise through convergent evolution suggesting both that plant and human MED19, despite being evolutionary distant, could adopt similar biochemical principles for their biological activities.

Materials and Methods

Arabidopsis thaliana materials, preparation of constructs, and transgenic plants and growth conditions

Arabidopsis thaliana ecotype Columbia-0 (Col-0) was used as the wild-type (WT). Mutants, *med19a-1* (SALK_037435), *med19a-2* (SALK_034955) and *ore1* (SALK_090154) were acquired from the Arabidopsis Biological Resource Centre (ABRC). *35S:ORE1-HA* (ORE1 OE#3) and *35S:GFP-MED19a* (MED19a OE#1) were described (Caillaud *et al.*, 2013; Park *et al.*, 2018).

In order to generate *MED19a-FLAG*, DNA sequences encoding 3× FLAG tag were added to the 3′ end of the PCR fragment for the MED19a coding sequence (CDS) and the fusion gene was cloned into pHUBQ10-DC (Jeong *et al.*, 2017) by LR cloning (Thermo Fisher Scientific, Waltham, MA, USA). Chimeric constructs *AtnHscMED19* and *AtnSccMED19* were chemically synthesized (Biobasic). To generate substitution mutants of *AtMED19a*, various *cMED19a* variants were synthesized (Bio Basic Inc., Markham, ON, Canada) and fused to *AtnMED19a* by restriction-free cloning. To generate *pMED19a:mEYFP-MED19a* complementation constructs, *MED19a* variants were introduced to the 3′ end of *pMED19a:mEYFP* by restriction-free cloning and transformed into pBA002a-DC (Zhang *et al.*, 2006) to acquire pBA002a-*pMED19a:mEYFP-MED19a* vectors. Primers used are listed in Table S1.

Constructs were introduced into Arabidopsis through *Agrobacterium*-mediated transformation by floral dip (Zhang *et al.*, 2006) and homozygous single insertion transgenic lines were used.

Plants were grown vertically under long day conditions (16 h : 8 h, light : dark) with 100 μmol m^{-2} s^{-1} light intensity. Seeds were sown on Murashige & Skoog (MS) medium plus 1% agar (Sigma-Aldrich).

Preparation of constructs for protein expression

pENTR containing the coding sequences (CDS) of various MED subunits were generated by PCR and cloned into MBP-DC-MYC vector by LR cloning (Thermo Fisher Scientific). Truncated *MED19a* constructs were generated by PCR reactions and cloned into pDONR221 vectors by BP cloning (Thermo Fisher Scientific). DNA sequences encoding N terminus and C terminus MED19a were generated from amino acid residues 1 to 112 and amino acid residues 113 to 221, respectively. These constructs were cloned into pMAL-DC-MYC by LR cloning (Thermo Fisher Scientific). Primers used are listed in Table S2.

For fluorescence-tagged proteins, CDS of indicated proteins were introduced into pET-28aSUMO-mCherry or pET-28aSUMO-mECFP vectors by restriction-free cloning. The protein expression constructs were transformed into *Escherichia coli* strain Rosetta (Novagen/Merck, Darmstadt, Germany).

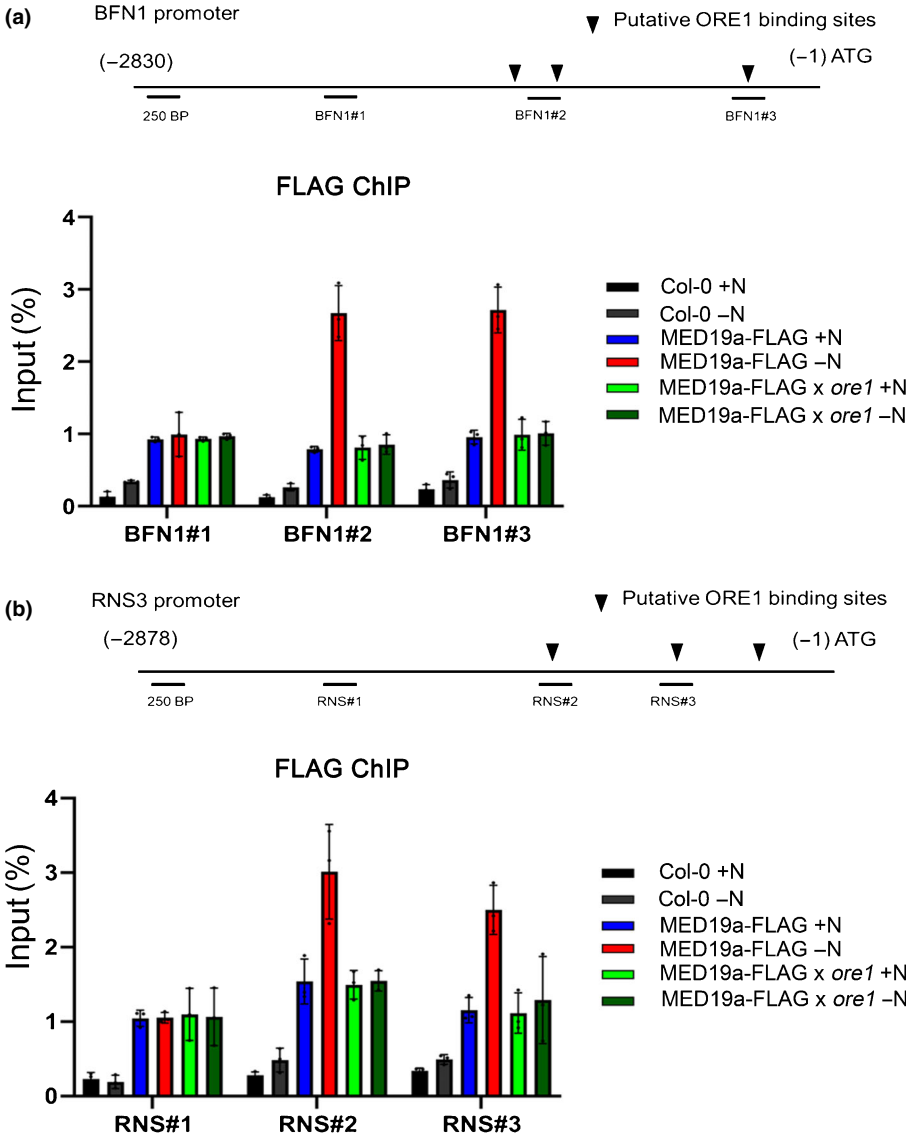

Fig. 2 Chromatin immunoprecipitation (ChIP) assay of MEDIATOR SUBUNIT (MED) 19a-FLAG enrichment on the promoters of *ORESARA1* (*ORE1*) target genes *BFN1* and *RNS3* under nitrogen sufficient (+N) and nitrogen deficient (−N) conditions in Arabidopsis. (a) Upper panel, schematic of *BFN1* promoter upstream of start codon (−1) ATG to (−2830). Arrows indicate putative *ORE1* binding sites. The regions probed are denoted as BFN#1, BFN#2 and BFN#3 which are 250 bp long. Lower panel, ChIP assay of *BFN1* promoter in the indicated genotypes under +N and −N conditions using FLAG-M2® agarose beads. (b) Upper panel, schematic of *BFN1* promoter upstream of the start codon (−1) ATG to (−2830). Arrows indicate putative ORE1 binding sites. The regions probed are denoted as BFN#1, BFN#2 and BFN#3 which are 250 bp long. Lower panel, ChIP assay of *RNS3* promoter in the indicated genotypes under +N and −N conditions using FLAG-M2® agarose beads. (a, b) Data are means ± SD. $n = 3$ (biologically independent repeats) and individual data points as overlays. The % input of MED19a-FLAG +N was set at 1 respectively.

−N phenotype assay and chlorophyll content quantification

Seventeen-days-old Arabidopsis plants grown vertically on MS plates without sucrose were transferred to 1% agar (Sigma-Aldrich) media containing modified Hoagland's solution +N or −N without sucrose (Hoagland and Arnon, 1950; Park *et al.*, 2018). Phenotypic observations were made between 17 and 21 d on −N medium. Leaves were sorted into three groups leaf 1 (L1), leaves 2 to 4 (L2 to L4) and leaves 5 (L5 to L7).

Total chlorophyll was extracted from leaf samples with 80% acetone overnight at 4°C and quantified with a 96-well plate reader (Tecan, Männedorf, Switzerland). Values were calculated according to a previous report (Porra *et al.*, 1989).

Confocal analysis of MED nuclear biomolecular condensates

Seventeen-days-old Arabidopsis seedlings expressing different fluorescence-tagged MED19a fusion proteins were treated on +N or −N media for 8 d. Roots from indicated plant were observed under a confocal microscope SP8 (Leica, Wetlzer, Germany) with a ×20 objective lens.

In vivo co-immunoprecipitation (Co-IP)

Co-immunoprecipitation was performed as described previously (Park *et al.*, 2019) with modifications. Briefly, 10-d-old seedlings of indicated transgenic lines on −N medium for 4 d were treated with 50 μM MG132, a proteasomal inhibitor, (Cat no: 474 790; Merck, Darmstadt, Germany) for at least 16 h. Nuclei from treated plant materials were extracted (Fiil *et al.*, 2008) for Co-IP assay. Proteins were separated on SDS-PAGE and analyzed by Western blotting with α-HA (ProteinTech, Rosemont, IL, USA) and α-FLAG (Sigma-Aldrich) antibodies.

Recombinant protein expression and purification

Recombinant proteins expressed from *E. coli* were purified accordingly to previous reports (Park *et al.*, 2018, 2019) with modifications.

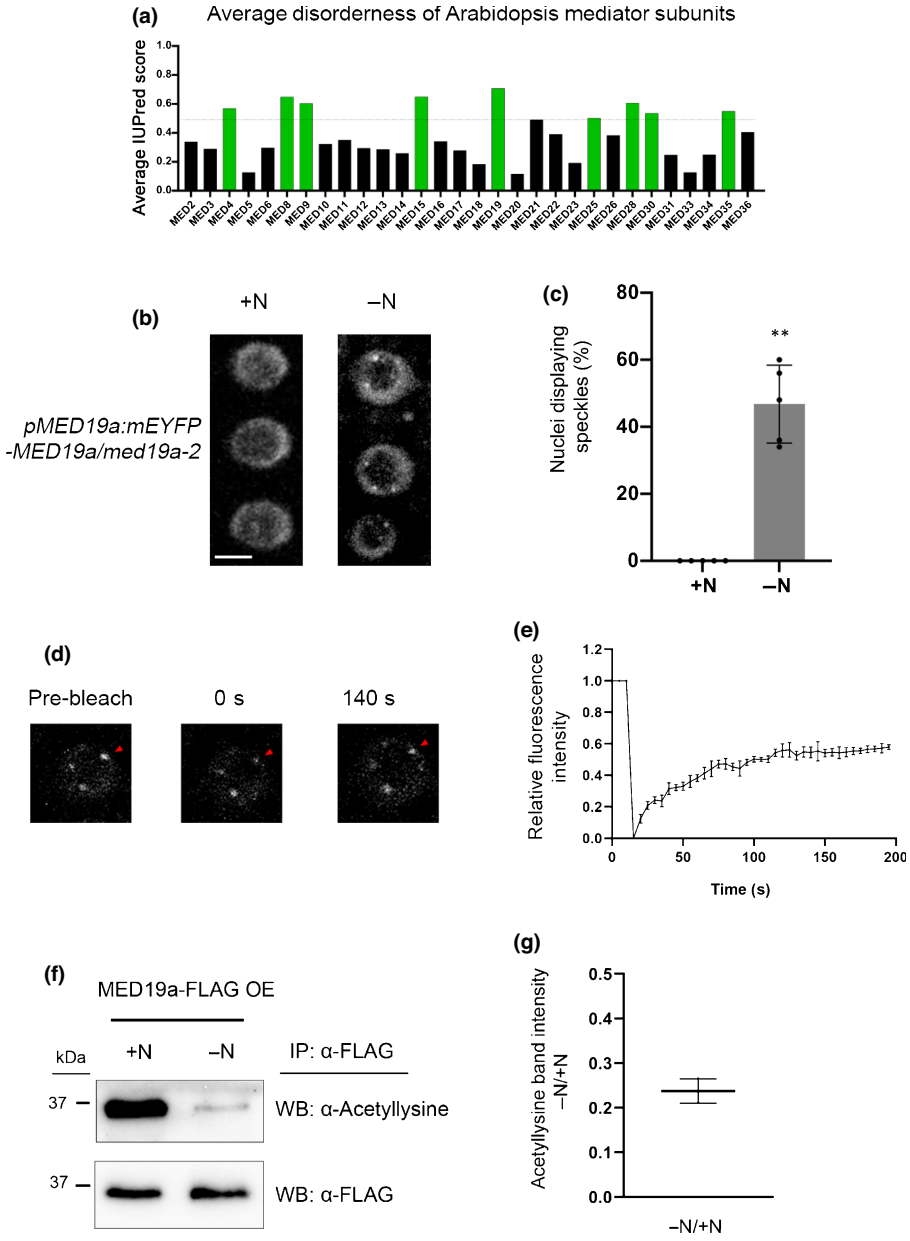

Fig. 3 Arabidopsis MEDIATOR SUBUNIT (MED)19a forms liquid-like condensates *in vivo* under nitrogen deficiency. (a) *In silico* IUPred prediction of the average disorderedness of Arabidopsis mediator subunits. Dotted line indicates average disorderedness of 0.5. Bars in green and black indicate disordered and nondisordered mediator subunits, respectively. (b) Representative root nuclei microscopy observation of 17-d-old *pMED19a:mEYFP-MED19a/med19a-2* seedlings treated on nitrogen sufficient (+N) and nitrogen deficient (−N) media for 8 d. Bar, 5 μm. (c) Quantification of root nuclei with speckles of 17-d-old *pMED19a:mEYFP-MED19a/med19a-2* seedlings treated on +N and −N media for 8 d. (d, e) Fluorescence recovery after photobleaching (FRAP) of 17-d-old *pMED19a:mEYFP-MED19a/med19a-2* seedlings treated on −N for 8 d. (d) Representative FRAP image. (e) FRAP quantification, $n = 7$ independent repeats. (f, g) *In vivo* acetyllysine detection of MED19a-FLAG OE plants treated under +N and −N for 8 d following α-FLAG immunoprecipitation and nuclear enrichment. (f) Upper panel, Western blot detection with α-acetyllysine. Lower panel, loading control Western blot detection with α-FLAG. (g) Ratio of with α-acetyllysine band intensity of −N/+N. Data represent mean ± SD. (b, c, d, e) Experiments were performed independently for five times with similar results. (c, e) Data are means ± SD. $n = 5$, individual data points as overlay. (c) Statistical significance: **, $P < 0.01$; two-tailed Student's *t*-test.

Briefly, induced cells were suspended in lysis buffer (50 mM Tris HCl pH 7.4, 200 mM NaCl, 1 mM $MgCl_2$, 1 mg ml^{-1} lysozyme, EDTA-free protease inhibitor cocktail (Roche), 10% glycerol) and sonicated (Qsonica, Newtown, CT, USA) on ice at 40% amplitude, 15 s on/30 s off, 15 cycles. Cell lysates were centrifuged at 21 000 ***g*** for 1 h (Beckman Coulter, Pasadena, CA, USA). The supernatant was mixed with equilibrated amylose (NEB, Ipswich, MA, USA) or glutathione Sepharose 4B (GE Healthcare, Chicago, IL, USA) or Ni-NTA (Bio Basic Inc.) beads correspondingly and manufacturers' instructions were followed to obtain purified proteins.

His-SUMO fluorescence-tagged proteins were cleaved with ULP1 enzyme and further purified to homogeneity with reverse Heparin chromatography (Cytiva, Marlborough, MA, USA), and 200 pg Superdex 16/600 size exclusion chromatography (Cytiva).

In vitro pull-down assay

In vitro pull-down assay was performed according to a previous report (Park *et al.*, 2018). Briefly, 500 ng of proteins were incubated in reaction buffer (20 mM Tris HCl pH 7.4, 150 mM NaCl, 0.2% glycerol, and protease inhibitor cocktail (Roche)) for 1 h at room temperature (RT). Equilibrated resins were then added into the mix which was further incubated for 1 h at RT. The resins with bound proteins were washed five times with the reaction buffer. Bound proteins were eluted by NuPAGE buffer (Thermo Fisher Scientific) containing lithium dodecyl sulfate (LDS) at pH 8.5 and incubated at 95°C for 5 min. Samples were analyzed by SDS-PAGE followed by Western blot analysis using α-HA and α-MYC antibodies (Santa Cruz Biotechnology, Dallas, TX, USA).

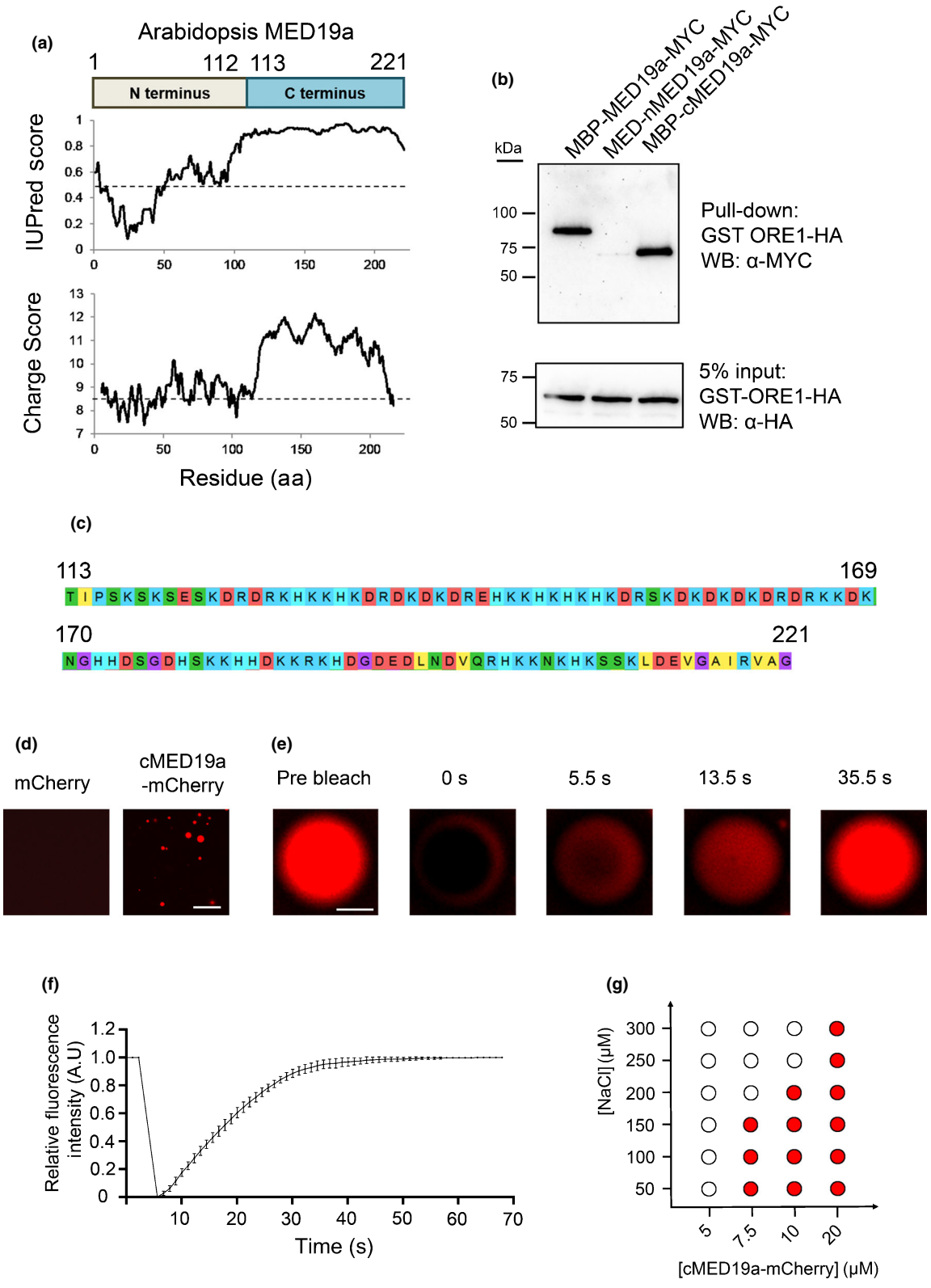

Yeast-two-hybrid (Y2H) assay

Coding sequence of *MED* subunits were cloned into pGBT9-DC via LR cloning reaction (Invitrogen) to generate BD-MED19a and BD-MED28. Coding sequence of *ORE1* was cloned into pGAD424-DC via LR cloning (Thermo Fisher Scientific) to generate AD-ORE1. Constructs were transformed into *Saccharomyces cerevisiae* strain AH109 according to the manufacturer's instructions (Clontech, Mountain View, CA, USA). Transformed cells were spotted on Sabouraud's dextrose (SD)/-

Fig. 4 Arabidopsis MEDIATOR SUBUNIT (MED)19a carboxyl terminus contains a mixed-charged intrinsically disordered region that is sufficient to interact with ORESARA1 (ORE1) and form biomolecular condensates. (a) *In silico* analysis of Arabidopsis MED19a protein. Upper panel, schematic of MED19a amino terminus and carboxyl terminus; numbers represent amino acid residues. Middle panel, disordered analysis of MED19a performed with IUPred. Lower panel, charged analysis of MED19a performed with Charge EMBOSS. (b) *In vitro* pull-down analysis of truncated MED19a proteins with ORE1. Upper panel, MBP-MED19a-MYC full-length and truncated proteins pull-down by GST-ORE1-HA via glutathione agarose beads, detected by α-MYC antibody. Lower panel, GST-ORE1-HA 5% input control detected α-HA antibody. (c) Amino acid sequence of Arabidopsis cMED19a. Numbers indicate amino acid residue of *Arabidopsis* MED19a. Colour code of amino acids: proline, lysine and arginine in blue; histidine in cyan; serine, threonine, asparagine and glutamine in green; valine, isoleucine, leucine and alanine in yellow. (d) *In vitro* droplet assay of indicated proteins at 10 μM concentration in 20 mM Tris HCl pH 7.4, 200 mM NaCl, 10% (w/v) PEG8000. Images were taken with a ×10 objective lens. Bar, 30 μm. (e) Representative images of 10 μM cMED19a-mCherry condensates in 20 mM Tris HCl pH 7.4, 200 mM NaCl, 10% (w/v) PEG8000 following fluorescence recovery after photobleaching (FRAP) assay. Photobleaching occurred at time 0. Bar, 2 μm. (f) FRAP time-course recovery plot of cMED19a-mCherry. Data are means ± SD. $N = 6$. (g) Phase diagram of cMED19a-mCherry in 20 mM Tris, 10% PEG8000 (w/v) at indicated NaCl and protein concentrations. Red circle and white circle represent presence and absence of cMED19a-mCherry condensates, respectively, observed with a ×100 objective lens. (b, d, e, f, g) Data are representative of three independent experiments.

Ade/-His/-Leu/-Trp quadruple deficient medium to examine for protein–protein interaction.

RNA expression analysis

Ten-days-old seedlings were transferred from MS without sucrose to modified Hoagland's −N medium without sucrose and grown under normal light conditions for 7 d. Total RNAs were extracted using RNA mini kit (Qiagen). Reverse transcription (RT) was performed with 1 μg RNA using iScript cDNA synthesis kit (Bio-Rad) following the manufacturer's instructions. The cDNA solution was diluted (1 : 3) with nuclease-free water. Quantitative PCR (qPCR) was performed using SyBR Green (Bio-Rad) on Bio-Rad CFX96 real-time system for 40 cycles using qPCR primers for *BFN1*, *RNS3*, *SAG29*, *SINA2* and *VNI2* (Park *et al.*, 2018, 2019). Primer pairs used are listed in Table S3.

In vitro droplet assay and fluorescence recovery after photobleaching (FRAP)

Pure fluorescence-tagged proteins were added to the indicated concentration and a final buffer concentration of 20 mM Tris HCl pH 7.4, 200 mM NaCl, 10% (w/v) PEG8000 (Sigma-Aldrich), unless indicated. Droplets on the glass slide focal plane were imaged and analyzed for FRAP.

Fluorescence recovery after photobleaching was performed using CellSens software on an Olympus FV3000 confocal microscope equipped with a 1.42 numerical aperture (NA) ×100 oil-immersion objective lens. The droplets were scanned five times before photobleaching. Photobleaching was performed using 100% laser power and the photobleached region then was allowed to recover, with laser power attenuated to 1% intensity.

Chromatin immunoprecipitation (ChIP) assay

Chromatin immunoprecipitation was performed according to previous reports (Fiil *et al.*, 2008) with minor modifications. In brief, 3 g of shoot materials were harvested and crosslinked with formaldehyde. Nuclei were isolated (Fiil *et al.*, 2008) followed by DNA shearing by sonication. Equilibrated FLAG-M2® (Sigma-Aldrich) beads were added to immunoprecipitate FLAG tagged protein-DNA complex. After reverse crosslinking DNA materials were purified using a DNA extraction kit (Qiagen) and bound DNA was eluted with nuclease-free water. Percentage input of ChIP samples against 1% input was measured with 40 cycles of qPCR using SyBR Green (Bio-Rad) on the Bio-Rad CFX96 real time system. Primer pairs are listed in Table S4.

In vivo acetyllysine quantification by Western blotting

Seventeen-days-old MED19a-FLAG OE seedlings were treated on +N and −N conditions for 8 d. On Day 7, samples were vacuum-infiltrated with the proteasomal inhibitor MG132 (50 μM; Merck, 474 790) and 5 g of samples were harvested on the next day. Nuclear fraction was isolated according to previous report (Fiil *et al.*, 2008) followed by immunoprecipitation with FLAG-M2® resins. The immunoprecipitated MED19a-FLAG proteins were analyzed on SDS-PAGE followed by Western blot with antibody against acetylated-lysine (Cell Signalling Technology, Leiden, the Netherlands) and FLAG-M2® (Sigma-Aldrich). Raw band intensities were quantified by ImageJ software. Normalized acetyllysine band intensities were obtained by dividing the raw band intensity of the +N and −N acetyllysine bands against respective input FLAG bands. The band intensity ratio of MED19a acetyllysine levels under −N to +N was derived by dividing the normalized acetyllysine intensities of −N by those of +N.

In vitro chemical lysine acetylation of cMED19a-mCherry

Chemical lysine acetylation of cMED19a-mCherry was based on a previous report (Guo *et al.*, 2021). Briefly, purified cMED19a-mCherry was acetylated by the addition of acetate anhydride and pyridine for 5 h. Lysine acetylated cMED19a-mCherry was visualized on a Coomassie stained SDS-PAGE and further purified by size exclusion chromatography.

RESULTS

MED19a is a positive regulator of −N induced senescence by associating with ORE1

In order to identify Arabidopsis mediator subunits that could be involved in ORE1-dependent senescence, we screened several mediator subunit mutants for delayed senescence under −N. The

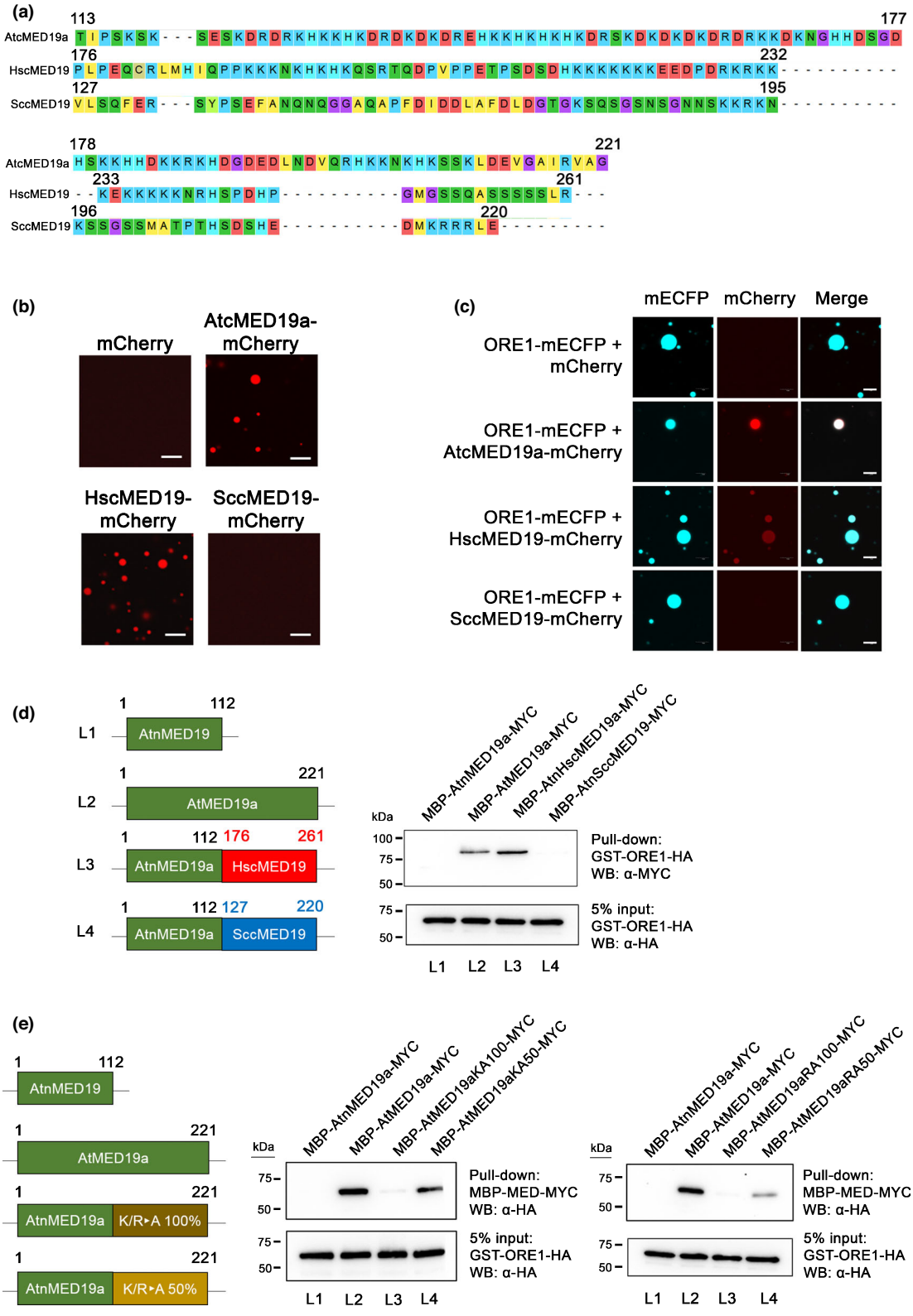

med19a mutants were analyzed further because of their comparable phenotypes with *ore1* (Fig. 1a). Both *med19a* mutants exhibited delayed senescence whereas MED19a OE plants displayed accelerated senescence phenotypes, phenocopying *ore1* and ORE1 OE#3, respectively, compared with WT (Fig. 1a). Chlorophyll contents in various leaf groups paralleled the −N phenotypes of the corresponding plants (Fig. 1b). We monitored −N inducible *ORE1* target genes (*BFN1*, *RNS3*, SAG29, *SINA1* and *VNI2*) (Rauf *et al.*, 2013; Park *et al.*, 2018, 2019) in the corresponding genotypes treated on −N medium (Fig. 1c). In WT

Fig. 5 Arabidopsis and human MEDIATOR SUBUNIT (MED)19a carboxyl termini contain a similar mixed-charge intrinsically disordered region necessary and sufficient to interact and form condensates with ORESARA1 (ORE1). (a) Sequence alignment of MED19 carboxyl terminus from *Arabidopsis thaliana* (AtcMED19), *Homo sapiens* (HscMED19) and *Saccharomyces cerevisiae* (SccMED19). Sequence alignment by MUSCLE performed by MEGA X. Numbers indicate amino acid residue of MED19 of corresponding organism. Colour code of amino acids: proline, lysine and arginine in blue; histidine in cyan; serine, threonine, asparagine and glutamine in green; valine, isoleucine, leucine, methionine and alanine in yellow; cytosine in flaxen; tyrosine in lime. (b) *In vitro* droplet assay of the indicated protein at 10 μM concentration in 20 mM Tris HCl pH 7.4, 200 mM NaCl, 10% PEG8000 (w/v). Images were taken with ×100 objective lens. Bar, 10 μm. (c) *In vitro* droplet recruitment assay of the indicated protein at 2 μM concentration in 20 mM Tris HCl pH 7.4, 200 mM NaCl, 10% PEG8000 (w/v). Images were taken with ×100 objective lens. Bar, 5 μm. (d) *In vitro* pull-down assay of MED19 chimeric proteins with ORE1. Left panel, schematic of the protein constructs used in the right panel. Numbers denote amino acid residues of Arabidopsis MED19a. Right-upper panel, chimeric MBP-MED19-MYC pull-down results by GST-ORE1-HA via glutathione agarose beads, detected by α-MYC antibody. Right-lower panel, 5% loading control for GST-ORE1-HA and detected by α-HA antibody. (e) *In vitro* pull-down assay of Arabidopsis MED19a lysine or arginine to alanine substitution mutant proteins with ORE1. Left panel, schematic of the protein constructs used in the middle and right panel. Numbers denote amino acid residues of Arabidopsis MED19a. Upper blots, pull-down of GST-ORE1-HA by MBP-MED19a-MYC substitution mutants via amylose resin beads, detected by α-HA antibody. Lower blots, 5% loading control for GST-ORE1-HA, detected by α-HA antibody.

plants, *ORE1* target genes were induced under −N but not +N, whereas *med19a-1*, *med19a-2* and *ore1* were unable to induce these genes under −N (Fig. 1c). By contrast, under −N treatment, MED19a OE displayed transcripts levels 2- to 5-fold higher than those in WT and 1.5- to 2-fold higher than those in ORE1 OE#3 (Fig. 1c). Furthermore, time-course qRT-PCR of WT plants treated on +N and −N revealed that both *MED19a* and *ORE1* were expressed in the shoot under −N (Fig. S1).

The parallel −N phenotype between *MED19a* and *ORE1* plants raises the question of the biochemical relationship of these two proteins. Fig. 1d shows that ORE1 interacted with MED19a and MED25 but not MED28 in Y2H assays. However, ORE1 bound to MED19a but not to MED25 nor MED28 *in vitro* pull-down assays (Fig. 1e), suggesting thatthe interaction of ORE1 with MED25 in yeast was indirect. *In vivo* immunoprecipitation of nuclear fraction from transgenic Arabidopsis plants treated under −N conditions confirmed the interaction of ORE1 and MED19a in Arabidopsis nuclei (Fig. 1f). The results indicated that MED19a and ORE1 physically associate *in vitro* and *in vivo* during −N.

The genetic relationship between *MED19a* and *ORE1* was investigated with various genetic crosses (Fig. 1g). We observed that *med19a* × *ore1* displayed delayed senescence phenotype and chlorophyll contents similar to those of *med19a* (Fig. 1g). The non-additive effect of the double mutant suggests that MED19a and ORE1 act in the same molecular pathway. Analysis of overexpressors in the reciprocal mutant backgrounds revealed that the accelerated senescence phenotypes in MED19a OE and ORE1 OE were blocked in *ore1* and *med19a* backgrounds, respectively (Fig. 1g,h). Furthermore, the double overexpressor MED19a OE × ORE1 OE displayed enhanced accelerated senescence (Fig. 1g,h). Transcript levels of *ORE1* target genes in the abovementioned genotypes under −N corroborated the phenotype and chlorophyll observations (Fig. 1f). The data demonstrated that the MED19a-ORE1 complex is necessary during −N induced senescence and the transcription of *ORE1* target genes under −N treatment.

ChIP assay was performed to examine the enrichment of MED19a-FLAG on the promoters of the two highly induced genes, *BFN1* and *RNS3* (Fig. 2). The putative ORE1 binding site has been described previously (Matallana-Ramirez *et al.*, 2013). Fig. 2(a,b) shows that MED19a was enriched between 1.5- and 3-fold on the promoters of both *BFN1* and *RNS3* under −N compared with +N in MED19a OE plants, and these enrichments were dependent on the presence of ORE1 binding sites in the probed regions BFN1#2, BFN1#3, RNS3#2 and RNS3#3. In the absence of ORE1 binding sites in probed regions BFN1#1 and RNS3#1, no enrichment of MED19a was observed (Fig. 2a, b). Consistently, MED19a enrichment on BFN1#2, BFN1#3, RNS3#2 and RNS3#3 were abolished in the *ore1* background, demonstrating that both ORE1 binding sites and ORE1 are required for MED19a enrichment on the promoters of *BFN1* and *RNS3* under −N (Fig. 2a,b).

MED19a undergoes −N inducible LLPS

Computer-based prediction of putative disordered protein structures of Arabidopsis mediator subunits revealed nine disordered mediator subunits (Fig. 3a). We analyzed the highly disordered mediator subunit MED19a for its ability to form nuclear condensates *in vivo* using *pMED19a:mEYFP-MED19a/med19a-2* seedlings. (Fig. 3). Fluorescence live-imaging of *pMED19a:mEYFP-MED19a/med19a-2* root tip revealed that mEYFP-MED19a was homogenously diffused in the nucleoplasm under +N (Fig. 3b). By contrast, mEYFP-MED19a formed discrete speckles in the nucleoplasm under −N (Fig. 3b). The number of nuclei displaying nuclear speckles was 46.8% at Day 8 of −N treatment, whereas no nuclei displayed nuclear speckles on +N treatment at all time points observed (Fig. 3c). The MED19a condensates were recoverable following photobleaching suggesting that MED19a proteins were in dynamic exchange with those in the nucleoplasm (Fig. 3d,e). These results demonstrated that MED19a forms inducible liquid-like nuclear condensates under −N but not +N conditions.

The abundance of lysine residues in MED19a (Fig. 4c) raises the possibility that MED19a inducible nuclear speckles are regulated by post-translation modifications (PTM) of lysine residues. It was shown previously that lysine acetylation negatively regulates LLPS of disordered proteins and MED19a was found to be lysine-acetylated on residues 119, 188 and 210 (Hartl *et al.*, 2017). Immunoprecipitation of MED19a-FLAG in plants treated on +N and −N for 8 d showed that lysine acetylation is significantly decreased under −N compared with +N by ≥ 4-fold suggesting that reducing lysine acetylation regulates MED19a LLPS *in vivo* (Fig. 3f,g).

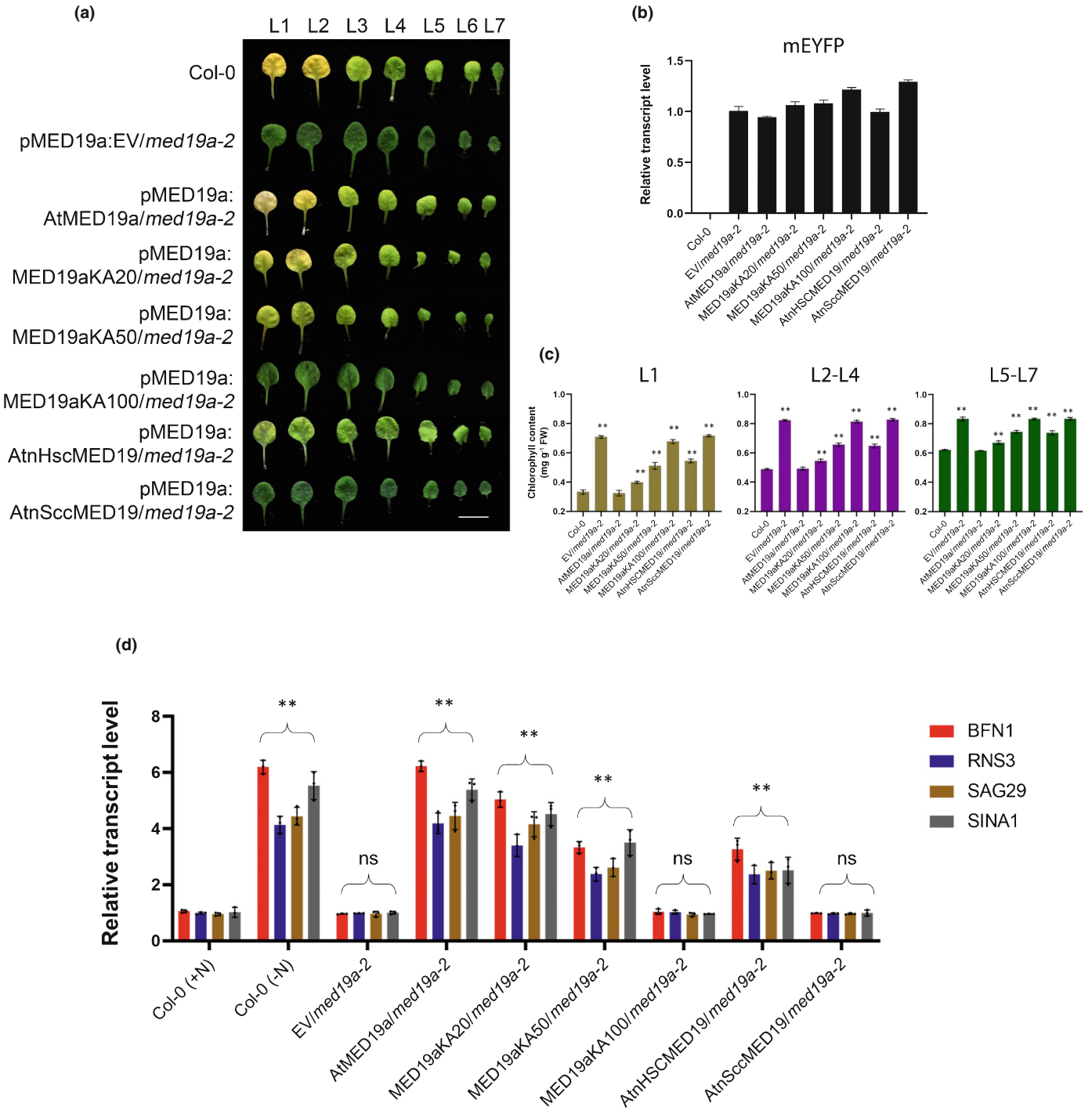

Fig. 6 Lysine enrichment in MEDIATOR SUBUNIT (MED)19 carboxyl terminus (cMED19) mixed-charged intrinsically disordered region (MC-IDR) is necessary to complement *med19a-2* under nitrogen deficient conditions. (a) Nitrogen deficiency induced senescence phenotype of 17-d-old Arabidopsis plants of wild-type (WT) (Col-0) and the indicated complementation lines in *med19a-2* background grown on nitrogen deficient (−N) medium for 21 d. EV, empty vector. All complementation constructs contain *mEYFP* upstream of *MED19a* start codon. Bar, 1 cm. (b) Quantitative reverse transcription (qRT)-PCR analysis of the yellow fluorescent protein (YFP) transcript levels. (c) Total chlorophyll content in different leaf groups of the indicated genotypes treated on −N medium. Leaf number, L. Asterisks indicate statistically significant difference compared with WT (Col-0). **, $P < 0.01$; one-way ANOVA, Dunnett *post hoc* analysis. (d) qRT-PCR analysis of *ORESARA1* (*ORE1*) target genes *BFN1*, *RNS3*, *SAG29* and *SINA1* of the indicated genotypes treated on nitrogen sufficient (+N) or nitrogen deficient (−N). The expression level of these genes in WT (Col-0 + N) was set at 1. Asterisks indicate statistically significant difference in various genotypes compared with WT (+N) for each respective gene. ns, no statistical difference, **, $P < 0.01$; two-way ANOVA analysis, Dunnett *post hoc* analysis. (c, d) Data are means ± SD. $n = 3$ (biologically independent repeats) and individual data points as overlays.

cMED19a MC-IDR is required to interact with ORE1 and sufficient to undergo LLPS

In order to elucidate the biochemical relationship between MED19a and ORE1, *in silico* analyses on the MED19a primary sequence was performed (Fig. 4a). Computer-based prediction of disordered protein structures by IUPred (Dosztanyi, 2018) suggested that MED19a contains an IDR from residues 113 to 221 on the carboxyl terminus. The cMED19a is highly charged as predicted by Charge EMBOSS, whereas MED19a amino terminus (nMED19a) is predicted to be structured and less charged (Fig. 4a).

Using *in vitro* pull-down assay, we showed that cMED19a but not nMED19a interacted with ORE1 (Fig. 4b). The cMED19a also harbors four highly enriched charged amino acid residues – lysine, arginine, histidine and aspartate (Fig. 4c) – suggesting that the MC-IDR of cMED19a probably associates with ORE1 through multivalent electrostatic interactions, which is a key molecular feature of phase separating systems (Li *et al.*, 2012; Hyman *et al.*, 2014; Wheeler *et al.*, 2016; Alberti, 2017).

In order to determine whether cMED19a is sufficient to undergo LLPS, a cDNA encoding MED19a-mCherry fusion protein was constructed and the expressed fusion protein was purified. *In vitro* droplet assay with the molecular crowding agent 10% (w/v) PEG8000 showed that 10 μM of cMED19a-mCherry, but not mCherry, was sufficient to undergo LLPS to form spherical homotypic condensates *in vitro* (Fig. 4d). The cMED19a-mCherry condensates displayed recovery following photobleaching (Fig. 4e,f) suggesting rapid dynamic exchange with the surrounding solution. Thorough analysis of cMED19a-mCherry LLPS revealed that the minimal concentration for cMED19a-mCherry to undergo LLPS was *c.*7.5 μM and the cMED19a-mCherry condensates were dispersed at high salt concentrations above 150 mM NaCl at 7.5 μM (Fig. 4g), suggesting that the homotypic condensates probably are driven by electrostatic interactions. Furthermore, *in vitro* chemical lysine acetylation of cMED19a-mCherry abolished LLPS, which is consistent with *in vivo* observation (Figs 3b,c,f,g, S4).

The MC-IDR of eukaryotic MED19 drives LLPS and interaction with ORE1

The molecular feature of Arabidopsis cMED19a resembles that of the human cMED19, which also is shown to be the site of interaction with several transcription factors in metazoans (Boube *et al.*, 2014; Immarigeon *et al.*, 2020). A previous report also described that eukaryotic cMED19 is intrinsically disordered in plants, metazoans and fungi (Nagulapalli *et al.*, 2016). To analyze eukaryotic cMED19, we aligned the protein sequences of *A. thaliana* cMED19a, *Homo sapiens* cMED19 and *Saccharomyces cerevisiae* cMED19 (Fig. 5a) as representatives of plants, metazoans and fungi, respectively. The alignment results showed that *A. thaliana* cMED19a and *H. sapiens* cMED19 both harbor the MC-IDR with enrichments in lysine, arginine, histidine and aspartate (Fig. 5a). On the contrary, *S. cerevisiae* cMED19 does not contain the similar enrichments in amino acid residues and does not possess any MC-IDR (Fig. 5a).

In order to investigate whether the MC-IDR in eukaryotic MED19 is a determinant of LLPS, we constructed *H. sapiens* cMED19 (HscMED19; aa 176 to 261) and *S. cerevisiae* cMED19 (SccMED19; aa 127 to 220) fused with mCherry (Fig. 5a). *In vitro* droplet assay with purified proteins at 10 μM revealed that *A. thaliana* cMED19a (AtcMED19a) and HscMED19 formed condensates but not SccMED19 (Fig. 5b), suggesting that MC-IDR in cMED19 drives LLPS *in vitro*.

In vitro droplet recruitment assay of purified proteins at 2 μM revealed that ORE1-mECFP was sufficient to form homotypic condensates and formed heterotypic condensates with AtcMED19a and HscMED19, but not with SccMED19 (Figs 5c, S2a). Furthermore, the difference in the strength of partitioning between the two MC-IDRs could be correlated to the length of the MC-IDR with AtcMED19a and HscMED19 being 108 aa and 85 aa, respectively (Figs 5a, S2a).

In vitro pull-down assay was performed to validate the interaction between the various eukaryotic cMED19s with ORE1 (Fig. 5d). We generated full-length chimeric constructs containing *A. thaliana* nMED19a with the two heterologous cMED19 (Fig. 5d). ORE1 was able to interact with AtnHscMED19 but not AtnSccMED19, which is consistent with *in vitro* droplet recruitment assay (Fig. 5d).

In order to decipher the biochemical determinants responsible for the interaction between cMED19 MC-IDR and ORE1, various AtcMED19a containing varying degrees of lysine-, arginine- or histidine-to-alanine substitutions were synthesized and fused to nMED19a to generate full-length AtMED19a mutants (Figs 5e, S2b). *In vitro* pull-down assays showed that AtMED19aKA100 and AtMED19aRA100 did not interact with ORE1 (Fig. 5e). Lysine and arginine residues previously were indicated to contribute to different types of electrostatic interactions (Gallivan & Dougherty, 1999). This suggests that both lysine and arginine residues on cMED19a contribute independently to the interaction with ORE1 through disparate electrostatic forces and is supported by the weak interaction with ORE1 displayed by AtMED19aKR100 (Fig. S2b). Histidine residues play critical roles in MED19a-ORE1 complex formation because ORE1 interaction was abolished in AtMED19aHA50 (Fig. S2b). It is possible that the basic aromatic residue could participate as positive charge donor and aromatic ring π donor. Our assays further revealed that ORE1 interaction was partially restored in AtMED19aKA50 and AtMED19aRA50 (Fig. 5e), demonstrating that the MED19a–ORE1 complex probably is stabilized by various weak multivalent interactions contributed by each charged residue.

The conserved enrichment of lysine, arginine, histidine and aspartate in MC-IDR raises the question of the biochemical contributions of these residues in promoting homotypic LLPS of AtcMED19a *in vitro*. All AtcMED19a mutant variants (WT, KA20, KA50, KA100, RA50, RA100, KR100, HA100 and DA50) together with HscMED19 and SccMED19 were purified and assayed for *in vitro* condensates at the indicated

New Phytologist

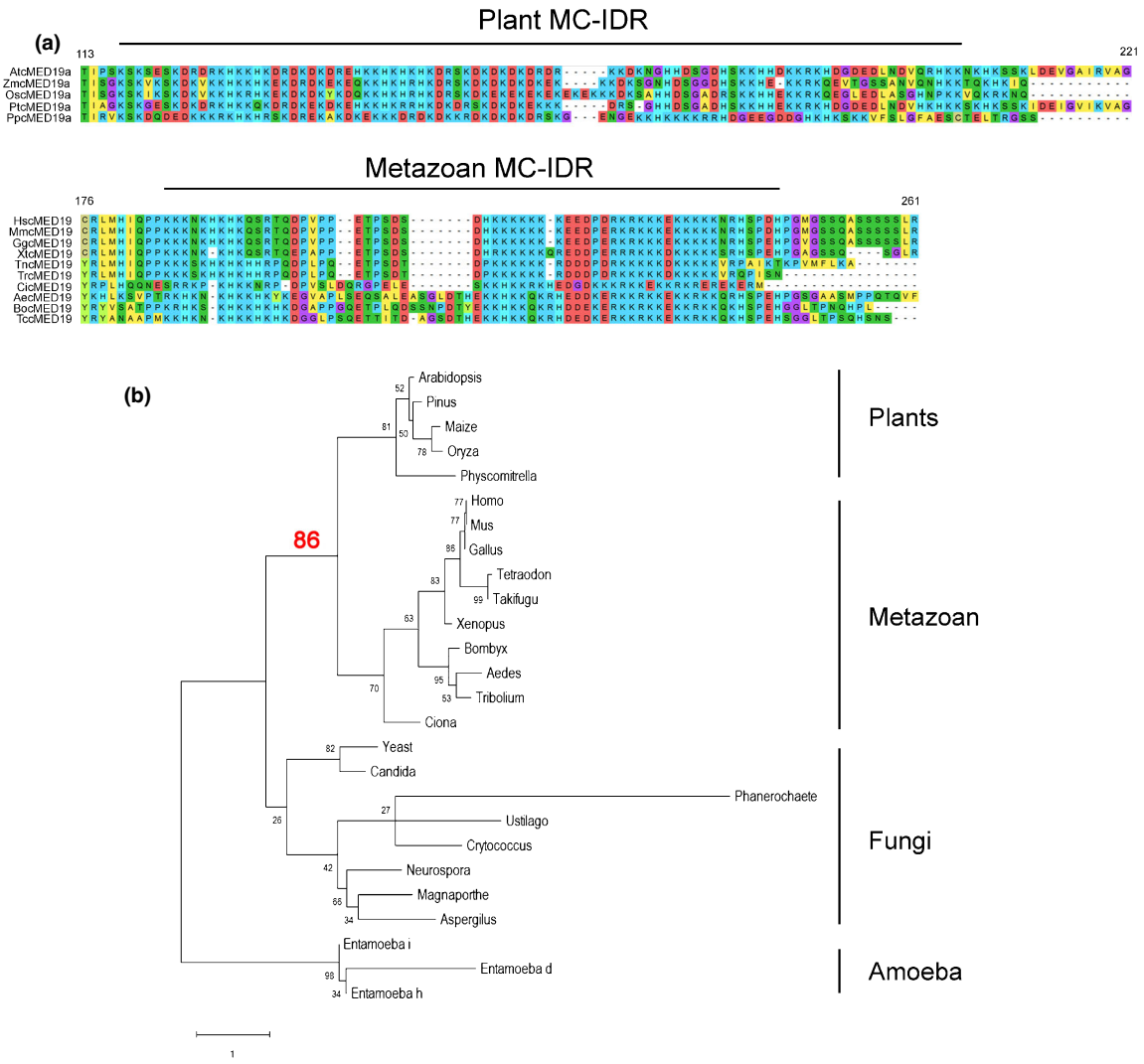

concentrations (Fig. S3). The results collectively revealed that MC-IDR is the biochemical determinant of MED19 LLPS and electrostatic interactions within the MC-IDR promote LLPS with lysine-aspartate residues probably forming cation-anion pairs and arginine-histidine residues forming cation-π pairs.

Fig. 7 MEDIATOR SUBUNIT (MED)19 carboxyl terminus (cMED19) mixed-charge intrinsically disordered region (MC-IDR) is highly conserved and probably evolved through convergent evolution in plants and metazoans. (a) Sequence alignment by MUSCLE performed by MEGA X. Upper panel, sequence alignment of cMED19 in plants. AtcMED19a, *Arabidopsis thaliana*; ZmcMED19a, *Zea mays*; OscMED19a, *Oryza sativa*; PtcMED19a, *Pinus taeda*; PpcMED19a, *Physcomitrella patens*. Lower panel, sequence alignment of cMED19 in metazoans. HscMED19, *Homo sapiens*; MmcMED19, *Mus musculus*; GgcMED19, *Gallus gallus*; XtcMED19, *Xenopus tropicalis*; TncMED19, *Tetraodon nigroviridis*; TrcMED19, *Takifugu rubripes*; CicMED19, *Ciona instestinalis*; AecMED19, *Aedes egypti*; BocMED19, *Bombyx mori*; TccMED19, *Tribolium casteneum*. Numbers indicate amino acid residue of Arabidopsis MED19a and human MED19 in upper and lower panels respectively. Colour code of amino acids: proline, lysine and arginine in blue; histidine in cyan; serine, threonine, asparagine and glutamine in green; valine, isoleucine, leucine, methionine and alanine in yellow; cytosine in flaxen; tyrosine in lime. (b) Phylogenetic analysis of cMED19 of the indicated eukaryotic groups. Global alignment of cMED19 of indicated organisms by MUSCLE performed by MEGA X, followed by analysis using the maximum likelihood method and JTT matrix-based model with bootstrap iterations, $n = 1000$. Numbers on branches indicate respective bootstrap value. The number in red and bold indicates the bootstrap value of the branch connecting plants and metazoans. (c) Working model of MED19a under nitrogen deficiency (−N) induced senescence. Upper panel, under nitrogen sufficient (+N) conditions, Arabidopsis cMED19a is enriched in acetyllysine and do not undergo liquid–liquid phase separation (LLPS). ORESARA1 (ORE1) is not expressed and the expression of senescence responsive genes is not activated. Lower panel, under −N conditions, acetyllysine levels in cMED19a is reduced, which promotes MED19a LLPS. ORE1 is expressed and MED19a interacts with ORE1 to activate the expression of senescence responsive genes, promoting −N induced senescence. Created with BIORENDER.

Lysine residues in cMED19 MC-IDR are necessary to complement *med19a* under −N conditions

In order to validate the biochemical observations, full-length cDNA encoding MED19a lysine to alanine mutants (MED19aKA100, MED19aKA50 and MED19aKA20), AtHscMED19 and AtSccMED19 described in Fig. 5 were separately fused in-frame downstream of the cDNA for *mEYFP*. The *MED19a* promoter was used to transcribe the fusion genes and the gene cassettes were transformed into the *med19a-2* background.

We analyzed transgenic complementation lines with equivalent *MED19a* transcript levels (Fig. 6b). Our results showed that the native promoter driven *mEYFP-MED19a* was functional under −N, which displayed similar levels of senescence phenotype and chlorophyll content compared with the WT (Fig. 6a,c). The ability of the lysine-to-alanine mutants to complement *med19a* was inversely correlated with the degree of lysine-to-alanine substitution. MED19aKA20 exhibited modest delayed senescence with a 13–25% increase in chlorophyll content (Fig. 6a,c). MED19aKA50 was sufficient to complement *med19a* partially by displaying a weak senescence phenotype with 20–50% chlorophyll content higher than that of MED19aKA20. MED19aKA100 exhibited delayed senescence and chlorophyll content similar to those of the empty vector (EV) in *med19a-2* background control, implying that MED19aKA100 was nonfunctional and unable to complement *med19a*. Complementation analysis of AtnHscMED19 and AtnSccMED19 in the *med19a* background demonstrated that the AtnHscMED19 chimeric protein was partially functional whereas AtnSccMED19 was nonfunctional (Fig. 6a,c). The AtnHscMED19 complementation line exhibited senescence phenotype and chlorophyll content similar to those of MED19aKA50. By contrast, the complementation line expressing AtnSccMED19 displayed delayed senescence with chlorophyll content similar to those of the EV control and MED19aKA100 (Fig. 6a,c). Transcript analysis of the target genes of *ORE1* in the abovementioned genotypes supported the phenotypic observations (Fig. 6d). These results demonstrate the importance of the lysine residue in the MC-IDR of MED19a which participate in activating ORE1 target genes through weak multivalent interactions with ORE1.

cMED19 MC-IDR molecular features are highly conserved in plants and metazoans and could arise by convergent evolution

The ability of AtnHscMED19 to complement *med19a* raises the question of the conservation of cMED19 MC-IDR within the plant and metazoan phyla. MED19a is present in bryophytes, gymnosperm, monocots and dicots, but not in *Pterophyta* (Mathur *et al.*, 2011). We aligned the amino acid sequences of MED19 from various species to represent the evolutionary history of plants (Mathur *et al.*, 2011). Sequence alignment of plant cMED19 (Fig. 7a, upper panel) revealed that plant cMED19 is highly conserved and the MC-IDR feature is present in all of the species examined. We also aligned the amino acid sequences of MED19 from organisms in the metazoan phylum (Bourbon, 2008) and discovered that the MC-IDR feature also is strongly conserved in all of the species examined (Fig. 7a, lower panel). The strong conservation of the MC-IDR feature in cMED19 of plants and metazoans suggest that the MC-IDR plays important biological roles in these evolutionary distant eukaryotes.

In order to investigate the evolutionary history of cMED19, we aligned the protein sequences of various organisms from plants, metazoans, fungi and amoeba based on a previous report (Bourbon, 2008). The maximum likelihood tree, with amoeba phylum rooted as an outgroup, revealed that cMED19 from plants and metazoans formed one clade whereas cMED19 from fungi formed another (Fig. 7b). The bootstrap value of the node connecting plants and metazoans was 86, suggesting a high statistical significance that this node is probable (Fig. 7b). The result suggests that cMED19 in plants and metazoans could be evolutionarily related and could arise through convergent evolution.

Discussion

In *A. thaliana*, −N induced senescence is a highly controlled process whereby ORE1, a central component of this process, is tightly regulated at transcriptional, post-transcriptional and post-translational levels (Kim *et al.*, 2009; Li *et al.*, 2013; Park *et al.*, 2018, 2019). Despite this understanding, the molecular signalling components of −N induced senescence remained

sparse. Furthermore, the molecular mechanism by which ORE1 regulates RNA polymerase II activity for *ORE1* target genes expression during −N was unknown. In this study, we showed that MED19a associates with ORE1 for −N induced senescence. Phenotype, RNA and ChIP analyses demonstrated that the MED19a-ORE1 forms a functional transcriptional complex that is necessary to activate the expression of *ORE1* target genes during −N treatment (Figs 1, 2). In the *med19a* background, the expression of these genes was blocked even with ORE1 OE under –N, demonstrating that MED19a is a necessary component of ORE1 activity (Fig. 1). Additionally, MED19a forms −N inducible liquid-like nuclear speckles (Fig. 3) that probably are transcriptional condensates positively regulating the expression of *ORE1* target genes (Figs 1, 6).

The ability of disordered mediator subunits to form transcriptional condensates has been documented previously (Shu *et al.*, 2016; Boija *et al.*, 2018; Sabari *et al.*, 2018; Guo *et al.*, 2021). We uncovered that MED19a forms inducible nuclear condensates *in vivo* under −N but not +N, and the percentage of nuclei displaying nuclear speckles was 46.8% on Day 8 of −N treatment (Fig. 3b,c). In comparison, *c.* 70% of nuclei formed SERRATE-containing dicing bodies involved in miRNA biogenesis (Xie *et al.*, 2021) and *c.* 17% of cells formed ELF3 speckles at 35°C as a form of thermoresponsive adaptation (Jung *et al.*, 2020). The ability of MED19a protein to undergo LLPS specifically under −N reflects the highly regulated nature of −N induced senescence (Oh *et al.*, 1996; Lim *et al.*, 2007; Feller *et al.*, 2008; Kim *et al.*, 2009; Hortensteiner & Krautler, 2011; Li *et al.*, 2013; Park *et al.*, 2018, 2019). Because senescence is a stepwise process, the leaf organ probably would commit a limited number of cells to undergo cell death at any given time to prevent toxicity to the organ (Fan *et al.*, 2009). The abundance of lysine residues in the MED19a MC-IDR raises the possibility that MED19a is regulated through lysine residue PTM. Our observations that MED19a lysine acetylation is decreased under −N compared with +N and that acetylation of lysine residues in cMED19a blocked LLPS *in vitro* (Figs 3f,g, S4) are consistent with the literature, whereby lysine acetylation acts as a switch to control LLPS conditionally (Hartl *et al.*, 2017; Kontaxi *et al.*, 2017; Owen & Shewmaker, 2019; Ukmar-Godec *et al.*, 2019).

Based on our results, we propose the following working model (Fig. 7c). Under +N conditions, lysine-acetylated MED19a is homogenously diffused in the nucleoplasm and there is no induction of *ORE1* target genes. Under −N conditions, MED19a lysine acetylation is reduced and undergoes −N induced LLPS to form MED19a transcriptional condensates that recruit ORE1. These MED19a-ORE1 condensates promote the expression of ORE1 target genes that are effectors of −N induced senescence (Fig. 7c).

Besides lysine residues, the cMED19a MC-IDR also is enriched in arginine, histidine and aspartate residues (Fig. 4c). Detailed biochemical analysis uncovered the molecular grammar of MC-IDR homotypic LLPS and heterotypic LLPS with ORE1, whereby various weak multivalent electrostatic forces such as charge–charge and cation-pi interactions driven by these residues are collectively necessary for interaction with ORE1, homotypic and heterotypic LLPS (Figs 4, 5e, S2b, S3).

ORE1 activity is reported to be enhanced by phosphorylation on ORE1-IDR. ORE1 phosphorylation by CPK1 provides the transcription factor with additional negatively charged sites which could potentially enhance the availability of charge–charge contacts between MED19a and ORE1 to facilitate greater activity of MED19a-ORE1 complex (Durian *et al.*, 2020). Hence, the specificity of MED19a interaction could be attributed to the collective strength of the various weak multivalent interactions, which is a recurring theme of considerable research interest (Scheepers & Prins, 2020).

Metazoan cMED19, that was reported to be necessary to interact with homeodomain transcription factors (Boube *et al.*, 2014; Immarigeon *et al.*, 2020), also harbors the MC-IDR molecular signature that is enriched in the same amino acid residues (Fig. 5a). Interestingly, immunostaining of MED19a in human cells, reported on Protein Altas, revealed that MED19 were localized into discrete nuclear speckles in cancer cell lines, suggesting that both plants and human MED19 can undergo LLPS. Our detailed biochemical analysis showed that the cMED19 MC-IDRs from plants and human are sufficient to drive LLPS at physiological concentrations (Figs 4b, S3).

The ability of AtnHscMED19, but not AtnSccMED19, to partially complement *med19a* further broadens the implications of our findings (Fig. 6). MED19 MC-IDR is highly conserved within plants and metazoans (Fig. 7a). Phylogenetic analysis of various eukaryotic cMED19 sequences revealed that plant and human cMED19 are closely related in sequence, whereas fungi and amoeba are evolutionarily distant (Fig. 7b). By contrast, the molecular clock suggested that fungi and metazoans shared a common ancestor 1481 to 900 Myr ago (Ma), whereas plants-fungi-metazoans diverged *c.* 1600 Ma (Douzery *et al.*, 2004; Peterson & Butterfield, 2005). The disparity between the phylogenetic tree of cMED19a (Fig. 7b) and the phylogeny of eukaryotes implies that cMED19 MC-IDR could be a result of convergent evolution. The convergence of MC-IDR in these evolutionarily distant multicellular eukaryotes also suggests that the pathway to multicellularity from unicellular eukaryotes could involve cMED19 MC-IDR. Gain-of-function analysis using multicellularity assays such as multicellular snowflake yeast and *Chlamydomonas reinhardtii* model systems could elucidate the function role of cMED19 MC-IDR in establishing complex multicellular organisms that could guide efforts in synthetic biology (Ratcliff *et al.*, 2013, 2015).

Recently, the mammalian MED19 was found to interact with PPARγ transcription factor to regulate adipogenesis and white adipose tissue maintenance (Dean *et al.*, 2020). It is conceivable that the metazoan MC-IDR could play critical roles in specific transcription factor interaction and phase separation. Human MED19, also known as LUNG CANCER METASTASIS RELATED 1 (LCMR 1), is overexpressed in many cancer cell types and facilitates cancer cell survival (Zhu *et al.*, 2013; Zhang *et al.*, 2019). Aberrant phase separation could be a cause for cancer. For example, the aberrant chimeric allele NUP98-HOXA9, generated by chromosomal translocation in various leukaemia subtypes, forms carcinogenic transcriptional condensates that upregulate leukemia-associated oncogenes (Ahn *et al.*, 2021).

Hence, understanding the evolutionary forces that drive the usage of MC-IDR in plant and metazoans MED19 could uncover broader biological roles of MC-IDR in developmental processes and pathogenesis.

Acknowledgements

We thank Zhou Yu for discussion on LLPS and Luo Dahai for the ULP1 vector. This work was supported by core funding from the Temasek Life Sciences Laboratory and The Disruptive & Sustainable Technology for Agricultural Precision (DiSTAP), an interdisciplinary research group (IRG) of the Singapore MIT Alliance for Research and Technology (SMART) Centre supported by the National Research Foundation (NRF), Prime Minister's Office, Singapore under its Campus for Research Excellence and Technological Enterprise (CREATE) program.

Competing interests

None declared.

Author contributions

SLHC, I-CJ and N-HC designed the experiments; and SLHC, H-WW, HX, RMS and TY executed the experiments. All of the authors interpreted and discussed the data; and SLHC and N-HC wrote the manuscript.

ORCID

Steven Le Hung Cheng https://orcid.org/0000-0001-7783-7165
Nam-Hai Chua https://orcid.org/0000-0002-8991-0355
In-Cheol Jang https://orcid.org/0000-0001-9408-4273
Hui-Wen Wu https://orcid.org/0000-0001-7226-2251

Data availability

The data that support the findings of this study are available from the corresponding author upon reasonable request.

References

Adviento-Borbe MA, Pittelkow CM, Anders M, Kessel C, Hill JE, McClung AM, Six J, Linquist BA. 2013. Optimal fertilizer nitrogen rates and yield-scaled global warming potential in drill seeded rice. *Journal of Environmental Quality* **42**: 1623–1634.

Ahn JH, Davis ES, Daugird TA, Zhao S, Quiroga IV, Urya H, Li J, Storey AJ, Tsai YH, Keeley DP *et al.* 2021. Phase separation drives aberrant chromatin looping and cancer development. *Nature* **595**: 591–595.

Alberti S. 2017. The wisdom of crowds: regulating cell function through condensed states of living matter. *Journal of Cell Science* **130**: 2789–2796.

Boija A, Klein IA, Sabari BR, Dall'Agnese A, Coffey EL, Zamudio AV, Li CH, Shrinivas K, Manteiga JC, Hannett NM *et al.* 2018. Transcription factors activate genes through the phase-separation capacity of their activation domains. *Cell* **175**: 1842–1855.

Boube M, Hudry B, Immarigeon C, Carrier Y, Bernat-Fabre S, Graba Y, Bourbon HM, Cribbs DL. 2014. Drosophila melanogaster Hox transcription factors access the RNA polymerase II machinery through direct homeodomain binding to a conserved motif of mediator subunit Med19. *PLoS Genetics* **10**: e1004303.

Bourbon HM. 2008. Comparative genomics supports a deep evolutionary origin for the large, four-module transcriptional mediator complex. *Nucleic Acids Research* **36**: 3993–4008.

Caillaud MC, Asai S, Rallapalli G, Piquerez S, Fabro G, Jones JDG. 2013. A downy mildew effector attenuates salicylic acid-triggered immunity in Arabidopsis by interacting with the host mediator complex. *PLoS Biology* **11**: e1001732.

Canet JV, Dobon A, Tornero P. 2012. Non-recognition-of-BTH4, an Arabidopsis mediator subunit homolog, is necessary for development and response to salicylic acid. *Plant Cell* **24**: 4220–4235.

Dean JM, He A, Tan M, Wang J, Lu D, Razani B, Lodhi I. 2020. MED19 regulates adipogenesis and maintenance of white adipose tissue mass by mediating PPARgamma-dependent gene expression. *Cell Reports* **33**: 108228.

Dorone Y, Boeynaems S, Flores E, Jin B, Hateley S, Bossi F, Lazarus E, Pennington JG, Michiels E, Decker MD *et al.* 2021. A prion-like protein regulator of seed germination undergoes hydration-dependent phase separation. *Cell* **184**: 4284–4298.

Dosztanyi Z. 2018. Prediction of protein disorder based on IUPred. *Protein Science* **27**: 331–340.

Douzery EJ, Snell EA, Bapteste E, Delsuc F, Philippe H. 2004. The timing of eukaryotic evolution: does a relaxed molecular clock reconcile proteins and fossils? *Proceedings of the National Academy of Sciences, USA* **101**: 15386–15391.

Durian G, Sedaghatmehr M, Matallana-Ramirez LP, Schilling SM, Schaepe S, Guerra T, Herde M, Witte CP, Mueller-Roeber B, Schulze WX *et al.* 2020. Calcium-dependent protein kinase CPK1 controls cell death by in vivo phosphorylation of senescence master regulator ORE1. *Plant Cell* **32**: 1610–1625.

Fan SC, Lin CS, Hsu PK, Lin SH, Tsay YF. 2009. The Arabidopsis nitrate transporter NRT1.7, expressed in phloem, is responsible for source-to-sink remobilization of nitrate. *Plant Cell* **21**: 2750–2761.

Feller U, Anders I, Mae T. 2008. Rubiscolytics: fate of Rubisco after its enzymatic function in a cell is terminated. *Journal of Experimental Botany* **59**: 1615–1624.

Feng Z, Jia B, Zhang M. 2021. Liquid–liquid phase separation in biology: specific stoichiometric molecular interactions vs promiscuous interactions mediated by disordered sequences. *Biochemistry* **60**: 2397–2406.

Fiil BK, Qiu JL, Peterson K, Peterson M, Mundy J. 2008. Coimmunoprecipitation (co-IP) of nuclear proteins and chromatin immunoprecipitation (ChIP) from Arabidopsis. *CSH Protocol* **2008**: pdb prot5049.

Gallivan JP, Dougherty DA. 1999. Cation-pi interactions in structural biology. *Proceedings of the National Academy of Sciences, USA* **96**: 9459–9464.

Gramma V, Kontbay K, Wahl V. 2020. Crops for the future: on the way to reduce nitrogen pollution. *American Journal of Botany* **107**: 1211–1213.

Guo J, Wei L, Chen SS, Cai XW, Su YN, Li L, Chen S, He XJ. 2021. The CBP/p300 histone acetyltransferases function as plant-specific MEDIATOR subunits in Arabidopsis. *Journal of Integrative Plant Biology* **63**: 755–771.

Hartl M, Füßl M, Boersema PJ, Jost JO, Kramer K, Bakirbas A, Sindlinger J, Plöchinger M, Leister D, Uhrig G *et al.* 2017. Lysine acetylome profiling uncovers novel histone deacetylase substrate proteins in Arabidopsis. *Molecular Systems Biology* **13**: 949.

Have M, Marmagne A, Chardon F, Masclaux-Daubresse C. 2017. Nitrogen remobilization during leaf senescence: lessons from Arabidopsis to crops. *Journal of Experimental Botany* **68**: 2513–2529.

Hnisz D, Shrinivas K, Young RA, Chakraborty AK, Sharp PA. 2017. A phase separation model for transcriptional control. *Cell* **169**: 13–23.

Hoagland DR, Arnon DI. 1950. *The water-culture method for growing plants without soil.* (Circular (California Agricultural Experiment Station), 347. ed.). Berkeley, CA, USA: University of California, College of Agriculture, Agricultural Experiment Station. (Revision).

Hortensteiner S, Krautler B. 2011. Chlorophyll breakdown in higher plants. *Biochimica et Biophysica Acta* **1807**: 977–988.

Hyman AA, Weber CA, Julicher F. 2014. Liquid–liquid phase separation in biology. *Annual Review of Cell and Developmental Biology* **30**: 39–58.

Immarigeon C, Bernat-Fabre S, Guillou E, Verger A, Prince E, Benmedjahed MA, Payet A, Couralet M, Monte D, Villeret V *et al.* 2020. Mediator complex subunit Med19 binds directly GATA transcription factors and is required with Med1 for GATA-driven gene regulation in vivo. *The Journal of Biological Chemistry* **295**: 13617–13629.

Imran A, Hakim S, Tariq M, Nawaz MS, Laraib I, Gulzar U, Hanif MK, Siddique MJ, Hayat M, Fraz A *et al.* 2021. Diazotrophs for lowering nitrogen pollution crises: looking deep into the roots. *Frontiers in Microbiology* **12**: 637815.

Izumi M, Wada S, Makino A, Ishida H. 2010. The autophagic degradation of chloroplasts via rubisco-containing bodies is specifically linked to leaf carbon status but not nitrogen status in Arabidopsis. *Plant Physiology* **154**: 1196–1209.

Jeong JS, Jung C, Seo JS, Kim JK, Chua NH. 2017. The deubiquitinating enzymes UBP12 and UBP13 positively regulate MYC2 levels in jasmonate responses. *Plant Cell* **29**: 1406–1424.

Jung JH, Barbosa AD, Hutin S, Kumita JR, Gao M, Derwot D, Silva CS, Lai X, Pierre E, Geng F *et al.* 2020. A prion-like domain in ELF3 functions as a thermosensor in Arabidopsis. *Nature* **585**: 256–260.

Kim JH, Woo HR, Kim J, Lim PO, Lee IC, Choi SH, Hwang D, Nam HG. 2009. Trifurcate feed-forward regulation of age-dependent cell death involving miR164 in Arabidopsis. *Science* **323**: 1053–1057.

Kontaxi C, Piccardo P, Gill AC. 2017. Lysine-directed post-translational modifications of tau protein in Alzheimer's disease and related tauopathies. *Frontiers in Molecular Biosciences* **4**: 56.

Lafontaine DLJ, Riback JA, Bascetin R, Brangwynne CP. 2021. The nucleolus as a multiphase liquid condensate. *Nature Reviews. Molecular Cell Biology* **22**: 165–182.

Lai Z, Schluttenhofer CM, Bhide K, Shreve J, Thimmapuram J, Lee SY, Yun DJ, Mengiste T. 2014. MED18 interaction with distinct transcription factors regulates multiple plant functions. *Nature Communications* **5**: 3064.

Lee HH, Kim SU, Han HR, Hur DY, Owens VN, Kumar S, Hong CO. 2021. Mitigation of global warming potential and greenhouse gas intensity in arable soil with green manure as source of nitrogen. *Environmental Pollution* **288**: 117724.

Li P, Banjade S, Cheng HC, Kim S, Chen B, Guo L, Llaguno M, Hollingsworth JV, King DS, Banani SF *et al.* 2012. Phase transitions in the assembly of multivalent signalling proteins. *Nature* **483**: 336–340.

Li Z, Peng J, Wen X, Guo H. 2013. Ethylene-insensitive3 is a senescence-associated gene that accelerates age-dependent leaf senescence by directly repressing miR164 transcription in Arabidopsis. *Plant Cell* **25**: 3311–3328.

Lim PO, Kim HJ, Nam HG. 2007. Leaf senescence. *Annual Review of Plant Biology* **58**: 115–136.

Liu F, Xu Y, Chang K, Zi S, Liu Z, Qi S, Jia J, Zhang M, Crawford NM, Wang Y. 2019. The long noncoding RNA T5120 regulates nitrate response and assimilation in Arabidopsis. *New Phytologist* **224**: 117–131.

Lu X, Ye X, Zhou M, Zhao Y, Weng H, Kong H, Li K, Gao M, Zheng B, Lin J *et al.* 2021. The underappreciated role of agricultural soil nitrogen oxide emissions in ozone pollution regulation in North China. *Nature Communications* **12**: 5021.

Matallana-Ramirez LP, Rauf M, Farage-Barhom S, Dortay H, Xue GP, Droge-Laser W, Lers A, Balazadeh S, Mueller-Roeber B. 2013. NAC transcription factor ORE1 and senescence-induced BIFUNCTIONAL NUCLEASE1 (BFN1) constitute a regulatory cascade in Arabidopsis. *Molecular Plant* **6**: 1438–1452.

Mathur S, Vyas S, Kapoor S, Tyagi AK. 2011. The Mediator complex in plants: structure, phylogeny, and expression profiling of representative genes in a dicot (Arabidopsis) and a monocot (rice) during reproduction and abiotic stress. *Plant Physiology* **157**: 1609–1627.

Nagulapalli M, Maji S, Dwivedi N, Dahiya P, Thakur JK. 2016. Evolution of disorder in Mediator complex and its functional relevance. *Nucleic Acids Research* **44**: 1591–1612.

Oh SA, Lee SY, Chung IK, Lee CH, Nam HG. 1996. A senescence-associated gene of Arabidopsis thaliana is distinctively regulated during natural and artificially induced leaf senescence. *Plant Molecular Biology* **30**: 739–754.

Oh SA, Park JH, Lee GI, Paek KH, Park SK, Nam HG. 1997. Identification of three genetic loci controlling leaf senescence in Arabidopsis thaliana. *The Plant Journal* **12**: 527–535.

Owen I, Shewmaker F. 2019. The role of post-translational modifications in the phase transitions of intrinsically disordered proteins. *International Journal of Molecular Sciences* **20**: 5501.

Park BS, Yao T, Seo JS, Wong ECC, Mitsuda N, Huang CH, Chua NH. 2018. Arabidopsis NITROGEN LIMITATION ADAPTATION regulates ORE1 homeostasis during senescence induced by nitrogen deficiency. *Nature Plants* **4**: 898–903.

Park SH, Jeong JS, Seo JS, Park BS, Chua NH. 2019. Arabidopsis ubiquitin-specific proteases UBP12 and UBP13 shape ORE1 levels during leaf senescence induced by nitrogen deficiency. *The New Phytologist* **223**: 1447–1460.

Peterson KJ, Butterfield NJ. 2005. Origin of the Eumetazoa: testing ecological predictions of molecular clocks against the Proterozoic fossil record. *Proceedings of the National Academy of Sciences, USA* **102**: 9547–9552.

Porra RJ, Thompson WA, Kriedemann PE. 1989. Determination of accurate extinction coefficients and simultaneous equations for assaying chlorophylls a and b extracted with four different solvents: verification of the concentration of chlorophyll standards by atomic absorption spectroscopy. *Biochimica et Biophysica Acta* **975**: 384–394.

Ratcliff WC, Fankhauser JD, Rogers DW, Greig D, Travisano M. 2015. Origins of multicellular evolvability in snowflake yeast. *Nature Communications* **6**: 6102.

Ratcliff WC, Herron MD, Howell K, Pentz JT, Rosenzweig F, Travisano M. 2013. Experimental evolution of an alternating uni- and multicellular life cycle in *Chlamydomonas reinhardtii*. *Nature Communications* **4**: 2742.

Rauf M, Arif M, Dortay H, Matallana-Ramirez LP, Water MT, Nam HG, Lim PK, Mueller-Roeber B, Balazadeh S. 2013. ORE1 balances leaf senescence against maintenance by antagonizing G2-like-mediated transcription. *EMBO Reports* **14**: 382–388.

Riback JA, Zhu L, Ferrolino MC, Tolbert M, Mitrea DM, Sanders DW, Wei MZ, Kriwacki RW, Brangwynne CP. 2020. Composition-dependent thermodynamics of intracellular phase separation. *Nature* **581**: 209–214.

Sabari BR, Dall'Agnese A, Boija A, Klein IA, Coffey EL, Shrinivas K, Abraham BJ, Hannett NM, Zamudio AV, Manteiga JC *et al.* 2018. Coactivator condensation at super-enhancers links phase separation and gene control. *Science* **361**: eaar3958.

Scheepers MRW, van Ijzendoorn ILJ, Prins MWJ. 2020. Multivalent weak interactions enhance selectivity of interparticle binding. *Proceedings of the National Academy of Sciences, USA* **117**: 22690–22697.

Shu S, Lin CY, He HH, Witwicki RM, Tabassum DP, Roberts JM, Janizewska M, Huh SJ, Liang Y, Ryan J *et al.* 2016. Response and resistance to BET bromodomain inhibitors in triple-negative breast cancer. *Nature* **529**: 413–417.

Soutourina J. 2018. Transcription regulation by the Mediator complex. *Nature Reviews. Molecular Cell Biology* **19**: 262–274.

Ukmar-Godec T, Hutten S, Grieshop MP, Rezaei-Ghaleh N, Cima-Omori MS, Biernat J, Mandelkow E, Soding J, Dormann D, Zweckstetter M. 2019. Lysine/RNA-interactions drive and regulate biomolecular condensation. *Nature Communications* **10**: 2909.

Wheeler JR, Matheny T, Jain S, Abrisch R, Parker R. 2016. Distinct stages in stress granule assembly and disassembly. *eLife* **5**: e18413.

Woo HR, Kim JH, Nam HG, Lim PO. 2004. The delayed leaf senescence mutants of Arabidopsis, ore1, ore3, and ore9 are tolerant to oxidative stress. *Plant & Cell Physiology* **45**: 923–932.

Xie D, Chen M, Niu J, Wang L, Li Y, Fang X, Li P, Qi Y. 2021. Phase separation of SERRATE drives dicing body assembly and promotes miRNA processing in Arabidopsis. *Nature Cell Biology* **23**: 32–39.

Zavaliev R, Mohan R, Chen T, Dong X. 2020. Formation of NPR1 condensates promotes cell survival during the plant immune response. *Cell* **182**: 1093–1108.

Zhang X, Gao D, Fang K, Guo Z, Li L. 2019. Med19 is targeted by miR-101-3p/miR-422a and promotes breast cancer progression by regulating the EGFR/MEK/ERK signaling pathway. *Cancer Letters* **444**: 105–115.

Zhang X, Henriques R, Lin SS, Niu QW, Chua NH. 2006. Agrobacterium-mediated transformation of Arabidopsis thaliana using the floral dip method. *Nature Protocols* **1**: 641–646.

Zhu LJ, Yang WX, Chen ZW, Chen Y, Chen D, Zhang TH, Liao GQ. 2013. Disruption of mediator complex subunit 19 (Med19) inhibits cell growth and migration in tongue cancer. *World Journal of Surgical Oncology* **11**: 116.

Supporting Information

Additional Supporting Information may be found online in the Supporting Information section at the end of the article.

Fig. S1 Time-course analysis of *MED19a and ORE1* transcript during N deficiency in WT plants.

Fig. S2 Biochemical analysis of MC-IDR for ORE1 condensate formation and interaction.

Fig. S3 MC-IDR is the biochemical determinant of LLPS in MED19.

Fig. S4 *In vitro* chemical acetylation of cMED19a abolishes liquid–liquid phase separation.

Table S1 Primers used in generating transgenic plants.

Table S2 Primers used for generating protein expression constructs.

Table S3 Primers used for qRT-PCR.

Table S4 Primers used in ChIP assay.

Please note: Wiley Blackwell are not responsible for the content or functionality of any Supporting Information supplied by the authors. Any queries (other than missing material) should be directed to the *New Phytologist* Central Office.